Title: Orientation anisotropies in human visual cortex

Authors:

Damien J. Mannion[1,2], J. Scott McDonald[1], & Colin W.G. Clifford[1,2]

Affiliations:

1. School of Psychology, The University of Sydney, NSW, 2006, Australia
2. Australian Research Council Centre of Excellence in Vision Science

Running head: Orientation anisotropies in human visual cortex

Contact information:

Damien J. Mannion
School of Psychology
Brennan MacCallum Building (A18)
The University of Sydney, NSW, 2006, Australia
damienm@psych.usyd.edu.au

Abstract

Representing the orientation of features in the visual image is a fundamental operation of the early cortical visual system. The nature of such representations can be informed by considering anisotropic distributions of response across the range of orientations. Here, we used functional magnetic resonance imaging to investigate modulations in the cortical activity elicited by observation of a sinusoidal grating which varied in orientation. We report a significant anisotropy in the measured blood-oxygen level-dependent activity within visual areas V1, V2, V3, and V3A/B in which horizontal orientations evoked a reduced response. These visual areas and hV4 showed a further anisotropy in which increased responses were observed for orientations that were radial to the point of fixation. We speculate that the anisotropies in cortical activity may be related to anisotropies in the prevalence and behavioural relevance of orientations in typical natural environments.

Introduction

The spatial arrangement of the visual image contains important information about the external environment. Previous fMRI research has yielded differing accounts of how the activity in human visual cortex is modulated by the orientation of such spatial structure. The distribution of response magnitude for varied stimulus orientation has been reported to be anisotropic in V1 (Furmanski and Engel 2000; Furmanski et al. 2004; Swisher et al. 2010), anisotropic also in ventral retinotopic regions (Serences et al. 2009), or isotropic (Kamitani and Tong 2005; Yacoub et al. 2008). When present, the anisotropy has taken the form of either an increased response to horizontal and vertical orientations (Furmanski and Engel 2000; Furmanski et al. 2004), oblique orientations (Swisher et al. 2010), or an orientation intermediate to the cardinal and primary oblique orientations (Serences et al. 2009). Hence, the nature of the distribution of fMRI responses to varying stimulus orientation remains equivocal.

While such studies considered pattern orientation independent of position in the visual field, anisotropic response distributions have been reported across the early human visual system when pattern orientation is specified relative to the local visual field meridian (see Figure 1). Specifically, responses are enhanced when the local pattern orientation is coincident with the angular meridian (radial) compared to when it is tangential (Sasaki et al. 2006; Clifford et al. 2009). An important consequence of this meridian-relative anisotropy is that it confers difficulties in the interpretation of putative anisotropies in field-independent pattern orientation, particularly when the stimulus (Furmanski and Engel 2000; Furmanski et al. 2004) or analysis (Serences et al. 2009; Yacoub et al. 2008) is restricted to a subregion of the visual field. In this circumstance, inferences about anisotropies in field-independent orientation can be confounded with those in meridian-relative orientation; for example, a stimulus restricted to the vertical visual field meridian will produce responses in which only the vertical field-independent orientation is also a radial meridian-relative orientation.

The aim of the current study was to measure the distribution of visual system responses to varied pattern orientation by considering both field-independent and meridian-relative indices. We used fMRI to measure the blood-oxygen level-dependent (BOLD) response to a sinusoidal grating which varied in orientation and to map the preferred visual field meridia from within the early retinotopic regions of human visual cortex. We report the presence of significant anisotropies to both

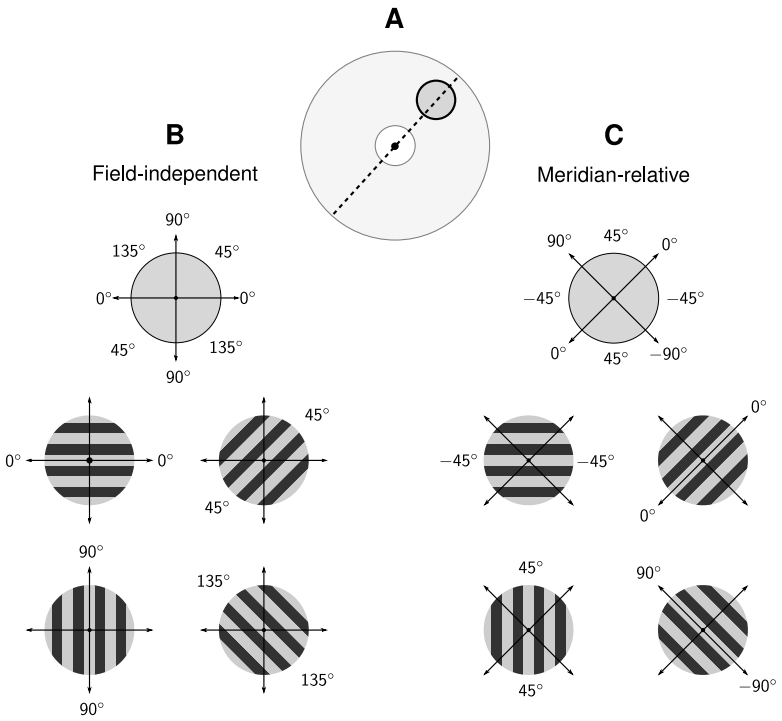

Figure 1. Illustration of field-independent and meridian-relative orientation indices. **A:** For an observer fixating on the central black dot, the annular region (light grey) represents the stimulated visual field and the circular region (dark grey) represents a responsive portion of the visual field for the current example. This responsive region lies along a meridian (dashed line) which connects it to the centre of gaze. **B:** The responsive region can be characterised in a coordinate system common to the entire visual field (*field-independent* orientation), in which a horizontal grating is identified as 0°, right-tilted oblique as 45°, vertical as 90°, and left-tilted oblique as 135°. **C:** The responsive region can also be characterised in a coordinate system which is rotated to align with the local meridian. For the example responsive region, this *meridian-relative* orientation system identifies a horizontal grating as −45°, right-tilted oblique as 0° (radial), vertical as 45°, and left-tilted oblique as ±90° (tangential).

field-independent and meridian-relative orientation from within visual areas V1, V2, V3, and V3A/B. While the form of meridian-relative anisotropy is consistent with previous reports of a preference for radial orientations, the anisotropy in field-independent orientation is characterised by a reduced response to horizontal orientations.

Materials and Methods

Subjects

Four experienced psychophysical observers participated in the current study. Each subject had received a recent optometric examination and all subjects, including those with clinically normal vision, wore customised corrective goggles during the experiment. Subjects gave their informed consent and the protocol was approved by a local ethics committee.

Apparatus

A Philips 3T scanner with a whole-head coil was used to conduct the MRI. Functional images were collected using a T_2^* sensitive, boustrophedon, field-echo echo-planar imaging pulse sequence (TR = 3s, TE = 32ms, flip angle = 90°, FOV = 69 × 192 × 192mm, matrix = 128 × 128, voxel size = 1.5mm isotropic). Images were acquired in 46 ascending interleaved slices in a tilted coronal plane covering the occipital lobes. Anatomical images were collected using a turbo field-echo protocol and consisted of whole-head scans in the axial and sagittal planes (voxel size = 1mm isotropic) and a high resolution partial-head coronal scan (voxel size = 0.75mm isotropic) to recover maximum detail in the occipital lobes.

Stimuli were displayed on a screen positioned behind the bore using a 5100MP projector (Dell Inc., Round Rock, TX) with a spatial resolution of 1024 × 768 pixels (1.12′ per pixel) and temporal resolution of 60Hz. The projector output was linearised via spline interpolation of luminance values measured with a SpectraScan PR-655 spectrophotometer (Photo Research Inc., Chatsworth, CA) and had a mean luminance of 275 cd / m^2. Subjects viewed the screen from a distance of 167cm via a mirror mounted on the head coil, giving a viewing angle of 19.0° × 14.3°. Stimuli were presented using PsychToolbox 3.0.8 (Brainard 1997; Pelli 1997). Behavioural responses were indicated via a LU400-PAIR response pad (Cedrus Corporation, San Pedro, CA). Analyses were performed using SPM5 (http://www.fil.ion.ucl.ac.uk/spm), mrVista (http://white.stanford.edu/software), and custom routines on Matlab 7.8 (The Mathworks, Natick, MA).

Stimuli

Separate stimulus sets were constructed to allow for modulation of pattern orientation and to perform retinotopic mapping. Pattern orientations were defined using a sinusoidal grating with a spatial frequency of 3.35 cycles / ° (Figure 2A), which is within a spatial frequency range shown to evoke high BOLD signal magnitudes in the early visual areas (Kay et al. 2008; Singh et al. 2000).. The grating was presented at full contrast within an annulus (0.75° inner radius, 7.2° outer radius, 0.35° raised cosine window at inner and outer edges) on a background equal to the mean grating luminance.

Retinotopic mapping was performed using a wedge that opened 45°, comprised of three 15° full contrast radial checkerboard strips, and extended to 7.2° eccentricity (Figure 2C; Larsson and Heeger 2006). The phase of each strip was incremented or decremented by 10° each frame, with the central strip moving in the opposite direction to its flankers. The wedge was presented on a background of mean luminance that was overlaid with a grid of several isopolar and isoeccentric lines to promote stable fixation (Hansen et al. 2007; Schira et al. 2007).

A coordinate convention was adopted for the visual field in which 0° was located at the right horizontal meridian and increasing angles advanced anti-clockwise. An analogous convention was applied for pattern orientation over a 180° range (0° = horizontal, 45° = right-tilted oblique, 90° = vertical, 135° = left-tilted oblique).

A small fixation marker was displayed at the centre of the screen throughout stimulus presentation, composed of an outer black circle 0.19° in diameter and an inner circle 0.09° in diameter that was either grey or white.

Design

We used continuous presentation paradigms to measure the BOLD response to modulations in pattern orientation (Yacoub et al. 2008) and to perform retinotopic mapping (DeYoe et al. 1996; Engel et al. 1997; Sereno et al. 1995). Each subject completed six pattern orientation runs, during which the grating orientation changed with each volume acquisition (3s) in stepwise 11.25° shifts (see Figure 2B). The direction of change alternated between clockwise and anti-clockwise over runs. The grating was absent in the first and last 250ms of each volume to prevent transients induced by abrupt changes in

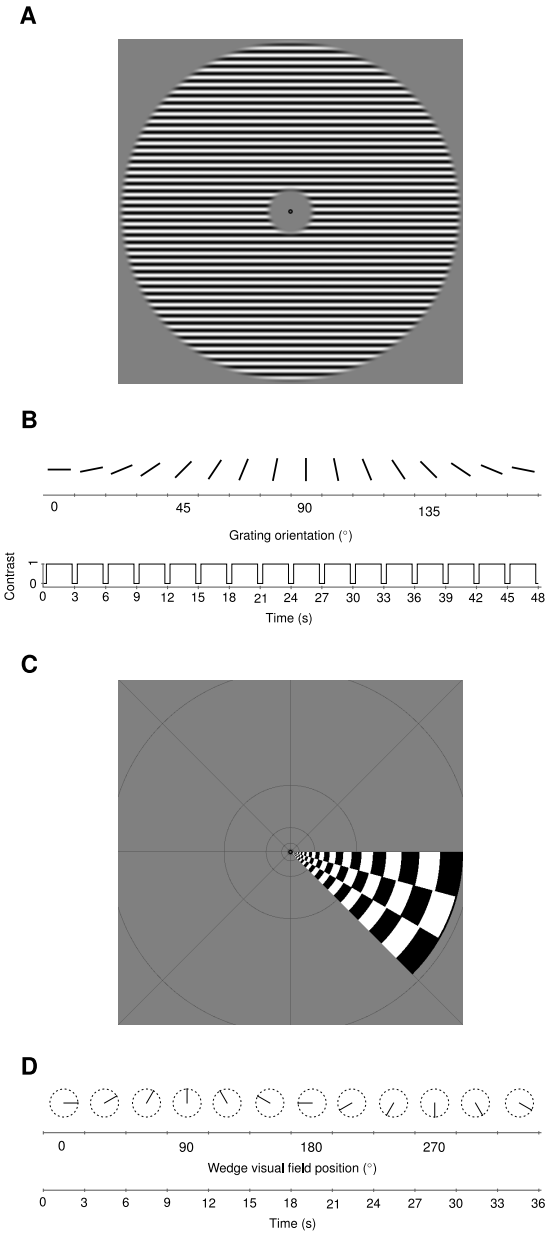

Figure 2. Illustration of orientation stimulus (**A**) and paradigm (**B**) and retinotopic mapping wedge stimulus (**C**) and paradigm (**D**). **A**: Pattern orientations were defined using a sinusoidal grating (horizontal / 0° in this example). **B**: Single cycle (48s) of the grating presentation sequence. The grating orientation changed in 11.25° stepwise shifts every 3s, with a 250ms period at the onset and offset of orientation change in which the grating is absent. The grating orientation advanced anti-clockwise, as shown in this example, on half the runs while it advanced clockwise during the remaining runs. **C**: Retinotopic mapping was performed using a polar wedge stimulus (located along the right horizontal / 0° visual field meridian in this example). **D:** Single cycle (36s) of the retinotopic mapping sequence. The location of the wedge in the visual field changed in 15° stepwise shifts every 1.5s (every second step shown in figure). The wedge location advanced anti-clockwise around the visual field, as shown in this example, on half the runs while it advanced clockwise during the remaining runs.

orientation, and the phase of the grating was updated with a new random value at 1Hz. Stimulus onset, offset, and phase changes were presented in a square-wave temporal cycle. A full orientation cycle was presented in 48 seconds (16 volumes), and eight complete cycles were completed in each run.

Each subject completed four retinotopic mapping runs, during which the polar angle of the wedge changed every 1.5s in stepwise 15° shifts (see Figure 2D). The direction of change alternated between clockwise and anti-clockwise over runs. The direction of motion in the wedge strips were assigned randomly at the beginning of each volume. A full polar wedge cycle was presented in 36 seconds (12 volumes), and 10 complete cycles were completed in each run.

To control fixation and attention, subjects performed a behavioural task throughout all runs in which they responded to increments in the luminance of the central fixation dot. Performance on the fixation task was quantified by the mutual information between increment onset and response, and was not significantly different (one-way ANOVA, $p > .05$) in windows around the principal grating orientations (0°, 45°, 90°, and 135°) across subjects.

Data pre-processing

Functional images were corrected for differences in slice acquisition time with the middle slice as reference. Between and within run subject movement was corrected and images were resliced using 4th degree B-spline interpolation. After discarding the first half-cycle of each run, a correction of +2 volumes (6s) was applied to compensate for the lag in the haemodynamic response. Timecourses from runs in which the stimulus advanced clockwise were temporally reversed, and were then combined with anti-clockwise runs to produce mean timecourses for pattern orientation and spatial polar angle.

A mean anatomical image was formed for each subject by combining the axial and sagittal whole-head scans and the coronal partial head scan. Before averaging, each anatomical image was inhomogeneity corrected (Manjòn et al. 2007), coregistered, and resampled to a voxel resolution of 0.75mm (isotropic) where necessary. Each subject's mean anatomical was then segmented using the automatic routines of mrGray (Teo et al. 1997) and ITKGray (Yushkevich et al. 2006, http://white.stanford.edu/software) followed by careful hand editing.

Analysis

The responses to the retinotopic mapping (polar wedge) stimulus were used to define the visual areas in early retinotopic cortex. Using mrVista, the preferred visual field polar angle of each voxel was estimated as the phase of the best-fitting sinusoid at the cycle frequency. The inplane voxels were then transformed onto a flattened representation of the cortical surface and the map of angular preferences was used to manually define areas V1, V2, V3, V3A/B, and hV4 based on the nomenclature and criteria of Larsson and Heeger (2006) and Wandell et al. (2007). To support appropriate area definition, eccentricity maps from previous studies with common subjects (Mannion et al. 2009) were also consulted. To restrict visual area definitions to stimulated portions of the visual field, voxels of low coherence (< 0.1) to the polar wedge stimulus and those within the fovea were excluded from further analysis. The visual area definitions are shown for each subject in Supplementary Figure 1.

The response to the pattern orientation stimulus cycle was calculated for each voxel within the identified visual areas. The pattern orientation timecourse was normalised by subtracting and then dividing by the mean voxel response, high-pass filtered (128s cutoff), and averaged over the eight cycles. For each voxel, this produced a 16-item vector of the evoked response to pattern orientation in 11.25° increments along the $[0°, 180°)$ interval. Voxels with a maximum signal change greater than 2 standard deviations above the mean maximum signal change for a given visual area were discarded from further analysis.

The voxels within each visual area were then binned according to their preferred spatial meridian (calculated by wrapping the preferred visual field polar angle at 180°), with bin centres corresponding to the 16 pattern orientations. The pattern orientation response vectors were then averaged across those voxels within a given visual area with a common spatial polar meridian bin. The data for each subject and visual area thus formed a 16×16 matrix (pattern orientation $\times$ spatial polar meridian). A schematic of this processing procedure is presented in Figure 3. Finally, this data matrix was sheared to transform the dimension indexing spatial polar meridian to index the circular distance between pattern orientation and spatial polar meridian (meridian-relative orientation).

A two-way repeated measures ANOVA was conducted for each visual area with subjects as a random factor and field-independent orientation and meridian-relative orientation as fixed factors

with 16 levels. As no statistical comparisons were applied across visual areas and each visual area was considered to comprise a separate statistical "family" (Ludbrook 1998), no correction for performing multiple ANOVAs (one for each of five visual areas) was applied. Violations of the assumption of sphericity were corrected by using Huynh-Feldt coefficients to reduce the effective degrees of freedom when assessing statistical significance.

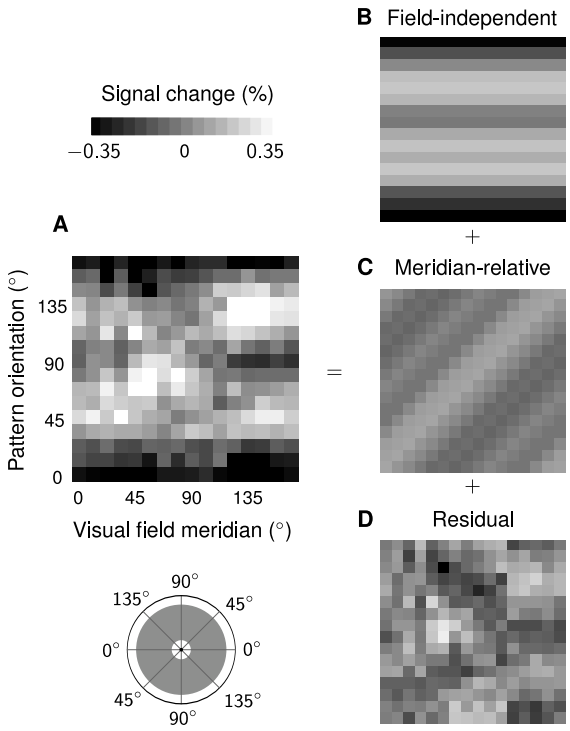

Figure 3. Analysis procedure illustrated with data from subject KS in visual area V1. **A**: Modulations in BOLD response to variations in pattern orientation were measured along visual field meridia, forming a 16×16 matrix. This matrix was modelled as consisting of modulations in response to field-independent pattern orientation (**B**) and meridian-relative orientation (**C**).
B: Modulations to field-independent pattern orientation were derived by averaging across all visual field meridia (matrix columns). **C**: Meridian-relative modulations were derived by averaging across cells with a common circular distance between pattern orientation and visual field meridian (matrix diagonals). **D**: The residuals reflected modulations unaccounted for by field-independent and meridian-relative factors.

Results

We measured the fMRI BOLD response from voxels within each of several retinotopically defined visual areas during observation of a sinusoidal grating which varied in orientation. The responses were binned according to the preferred spatial polar meridian of each voxel, defined using a rotating wedge stimulus, which allowed for the investigation of responses to both the grating orientation independent of position in the visual field and the conjunction between grating orientation and visual field meridian (see Figure 3). We performed a two-way repeated measures ANOVA (field-independent orientation × meridian-relative orientation) to investigate potential anisotropies in the measured BOLD signal across both field-independent and meridian-relative grating orientation.

The magnitude of BOLD activity was significantly anisotropic across field-independent orientation in areas V1, V2, V3, and V3A/B (V1: $F_{4.4,13.2} = 8.15, p = .001$; V2: $F_{15.0,45.0} = 7.71, p < .001$; V3: $F_{15.0,45.0} = 8.87, p < .001$; V3A/B: $F_{3.9,11.8} = 3.76, p = .034$), while there was no significant anisotropy in hV4 ($F_{10.4,31.1} = 1.28, p = .281$). As shown in Figure 4A, this anisotropy took the form of a reduction in BOLD activity during observation of a horizontal grating (0°). The anisotropy was consistent across visual areas, with each of V1, V2, V3, and V3A/B showing the lowest response to horizontal orientations. Area V1 also showed an apparent reduction in response to vertical orientations (90°) relative to those at the primary obliques (45°, 135°), while this anisotropy was not as clearly evident in areas V2, V3, and V3A/B.

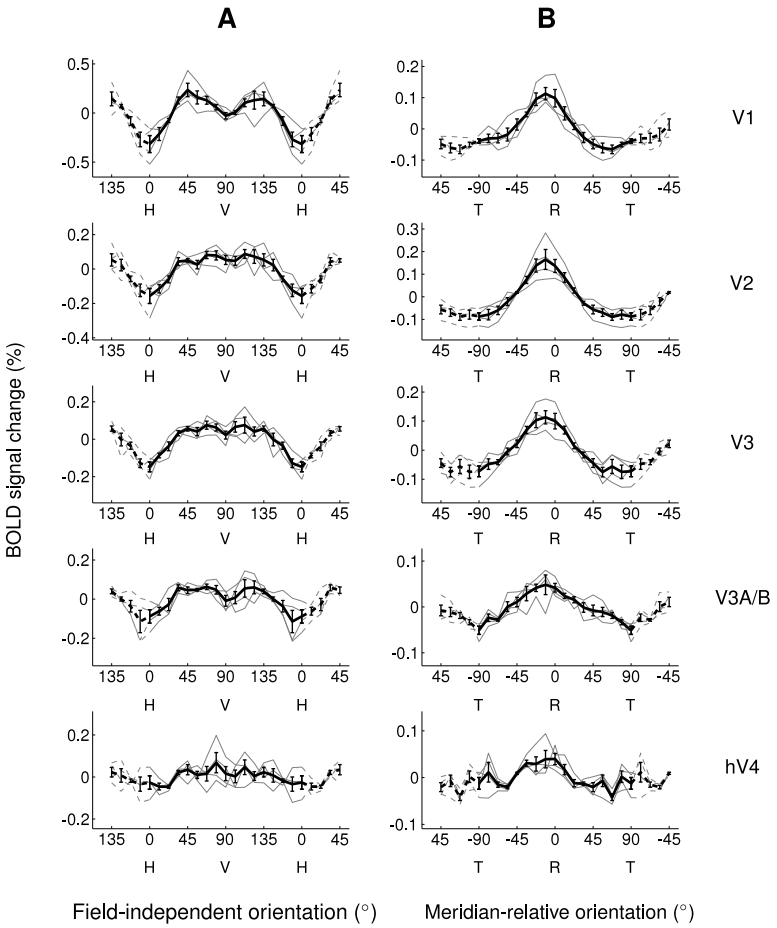

Figure 4. Modulation in BOLD response across the early visual areas to **A:** field-independent pattern orientation (0° = horizontal [H], 45° = rightwards tilt, 90° = vertical [V], 135° = leftwards tilt); **B:** meridian-relative orientation (0° = radial [R], ±90° = tangential [T]). All plots show mean over subjects ± SEM (thick black line) and individual subjects (thin grey lines), have an extra quarter cycle wrapped at each end (dashed segments), and are presented on ordinate scales that are unstandardised across plots.

The magnitude of BOLD activity was significantly anisotropic across meridian-relative orientation in all areas (V1: $F_{5.7,17.0} = 12.13, p < .001$; V2: $F_{1.6,4.7} = 16.43, p = .009$; V3: $F_{2.4,7.3} = 13.73, p = .003$; V3A/B: $F_{7.4,22.1} = 7.61, p < .001$; hV4: $F_{4.8,14.4} = 4.22, p = .015$). As shown in Figure 4B, the greatest BOLD responses were obtained when the pattern orientation and visual field meridian were near coincident (meridian-relative orientation $\sim 0°$), and the magnitude of response gradually reduced with increasing circular distance between the pattern orientation and the visual field meridian. This profile of

meridian-relative anisotropy was consistent across all the visual areas.

The magnitude of anisotropy, as defined by the range of the fMRI signal change across orientation, was lower for meridian-relative orientation relative to field-independent orientation. While this may be indicative of an increased strength of the field-independent orientation anisotropy in comparison with the anisotropy in meridian-relative orientation, it may also reflect the inevitable loss in precision when estimating meridian-relative orientation due to the reliance on retinotopic mapping in the current experiment.

There were no significant interactions in visual areas V1, V2, V3, and V3A/B (all $p > .05$), which may be suggestive of an independence between the observed field-independent and meridian-relative effects or may reflect insufficient statistical power to detect such interactions in the current experiment. While the interaction was significant in hV4 ($F_{225.0,675.0} = 1.27, p = .012$), further analysis revealed no clear pattern of factor level dependence on the responses to either field-independent or meridian-relative orientation. We speculate that the less precise visual field polar angle mapping of hV4 (see Supplementary Figure 1) may have restricted the ability to observe consistent meridian-relative anisotropies across the range of visual field meridia.

Discussion

We investigated modulations in the response of human visual cortex induced by both the orientation of an observed pattern and by the conjunction of pattern orientation and angular position in the visual field. Using fMRI, we identified the preferred visual field meridian of voxels within retinotopic regions of human visual cortex and then measured their responses to a sinusoidal grating which varied in orientation. We report an anisotropic distribution of responses to field-independent pattern orientation within areas V1, V2, V3, and V3A/B, with a form characterised by the lowest response to horizontal, intermediate at vertical, and highest at oblique orientations. We also report that when orientation is considered relative to angular position in the visual field, an anisotropic distribution of responses is observed in V1, V2, V3, V3A/B, and hV4 in which the greatest response is obtained when the pattern orientation and visual field meridian are parallel.

The functional role of anisotropies in the visual system can be informed by considering the structure of typical system input. The distribution of field-independent orientation content in typical natural scenes is anisotropic, with horizontal and vertical more prevalent than obliques (Coppola et al. 1998; Dragoi et al. 2001; Hansen and Essock 2004) and horizontal more prevalent than vertical (Hansen and Essock 2004). The apparent inversion of this distribution in the magnitude of response to field-independent orientation in the current study, most clearly evident in V1, suggests a representational strategy that is accommodative to anisotropies present in a typically observed scene (Essock et al. 2003). Such a strategy would allow for a redistribution of the anisotropic input structure, potentially leading to an isotropic representation of field-independent orientation (Essock et al. 2003). The presence of such a whitening mechanism would be consistent with those commonly thought to operate across spatiotemporal frequency (Dan et al. 1996; Field 1987; Webster and Miyahara 1997) and with the principle of efficient neural coding (Barlow 1961; Field 1987; Simoncelli 2003).

The measured fMRI activity has its substrate in changes in the excitatory and inhibitory balance within the collection of neurons sampled within each voxel (Logothetis 2008). Non-human neurophysiology indicates that the greatest number of cortical neurons respond to horizontal field-independent orientation, reduced at vertical, and the least at the obliques (Li et al. 2003). This numerical anisotropy suggests that an integrated population response would show strong levels of matching anisotropy in response to field-independent orientation, which would enhance the anisotropy of typical natural scenes (Essock et al. 2003; Hansen and Essock 2004). The clear departure from such a prediction in the field-independent orientation anisotropy in fMRI activity reported here suggests the presence of a mechanism that adjusts the contribution of neurons according to their preferred field-independent orientation (Essock et al. 2003; Hansen et al. 2003; Essock et al. 2009). Such a normalisation mechanism could be implemented by having orientation selectivity bandwidths which are inversely proportional to the numerical field-independent orientation anisotropy, as reported by Li et al. (2003), or by a gain-control process similar to those commonly considered to operate within the early cortical visual system (Hansen et al. 2003; Heeger 1992).

However, the meridian-relative anisotropy observed in the current study suggests that such a normalisation mechanism does not have universal application in the early visual system. Analyses of the meridian-relative orientation structure of natural scenes have revealed a preponderance of

orientations radial to the image centre (Bruce and Tsotsos 2006) and to the centre of simulated gaze (Rothkopf et al. 2009). Non-human neurophysiology has shown an over-representation of cortical neurons preferring radial meridian-relative orientations (Leventhal 1983) that is also present in the retina (Levick and Thibos 1982). The measured fMRI activity across meridian-relative orientation reported here corresponds to this profile of anisotropy, with radial orientations producing greater activity than tangential. Thus, the representation of meridian-relative orientation in the early visual system appears to reproduce and enhance the meridian-relative anisotropy present in typical system input.

The apparent differences in the representational strategy for field-independent and meridian-relative orientation may potentially be related to divergent behavioural relevance of the two indices. Redistribution of the field-independent anisotropy in a typical natural image would be an appropriate strategy where the relevance of features in the environment does not correspond to their prevalence. If there is no consistent relationship between feature relevance and field-independent orientation, this redistribution would allow an efficient isotropic representation of field-independent orientation (Essock et al. 2003; Hansen et al. 2003). Conversely, radial meridian-relative orientations have been associated with computations such as the establishment of geometric perspective (Bruce and Tsotsos 2006; Rothkopf et al. 2009) and optic flow (Geisler 1999; Lee 1980; Raemaekers et al. 2009), and thus a cortical representation that preserves the meridian-relative anisotropy may be behaviourally beneficial. Such optimisation of visual system anisotropies in accordance with ecological demands appears to be a common principle across species (O'Carroll et al. 1996).

The meridian-relative anisotropy reported here is consistent with the increased behavioural sensitivity for radial meridian-relative orientations (Rovamo et al. 1982; Sasaki et al. 2006; Westheimer 2003a). However, the form of field-independent anisotropy highlights a difficulty in establishing the link between behavioural performance and neural activity (Teller 1984). Sensitivity to field-independent orientation is superior, across a variety of behavioural indices, at horizontal and vertical compared to the obliques—the oblique effect (Appelle 1972). This psychophysical anisotropy is inconsistent with the anisotropy in field-independent orientation reported here, in which horizontal orientations produce the lowest levels of activity, suggesting that the magnitude of evoked activity in the early visual system does not necessarily determine behavioural sensitivity (Westheimer 2003b).

Furthermore, an over-representation of horizontal and vertical detecting mechanisms is insufficient to explain the dependence of the oblique effect on the image spectrum (Essock et al. 2003, 2009; Hansen and Essock 2006) and complexity (Jenkins 1985; Wilson et al. 2001). Further research is thus required to clarify the relationship between field-independent orientation anisotropies evident in behavioural performance and those evident in measures of neural activity.

The nature of the anisotropies reported in the current study may be continent upon the particular choice of stimulus attributes and behavioural task. Both field-independent and meridian-relative anisotropies have been shown to vary with spatial frequency and eccentricity (e.g. Heeley and Timney 1988; Li et al. 2003; Raemaekers et al. 2009; Rovamo et al. 1982; Vandenbussche et al. 1986). However, such interactions typically involve a modulation of the strength or existence, rather than the form, of the anisotropy. Furthermore, the reported profiles of anisotropy may be contingent upon the task performed by the observer. In this experiment, having observers complete a task at fixation that was unrelated to the experimental stimulus allowed us to limit the influence of eye movements and shifts in attention on the measured BOLD responses. However, it is possible that requiring observers to complete a task involving the stimulus (such as discrimination or change detection) may engage different neural mechanisms and result in alterations to the form of evoked orientation anisotropy (Williams 1982).

In conclusion, we report the presence of significant anisotropies in the response of human visual cortex to pattern orientation. Consideration of field-independent orientation revealed anisotropic responses within V1, V2, V3, and V3A/B, characterised by a decreased response to horizontal orientations, intermediate response to vertical orientations, and the highest response to oblique orientations. When orientation was considered relative to angular position in the visual field, meridian-relative anisotropies were observed in areas V1, V2, V3, V3A/B, and hV4 in which radial orientations produced greater responses than those that were tangential. We speculate that such anisotropies are related to the behavioural relevance of feature orientation, with anisotropic field-independent orientation content in typical scenes being redistributed via a neural normalisation process to produce an efficient isotropic representation, while anisotropic meridian-relative orientation content is maintained in the cortical representation. Future research is required to elucidate the precise nature of the field-independent redistributive process and to directly investigate

the cortical representation of the orientation structure of natural environments.

Acknowledgements

We thank the radiography team at St. Vincent's Hospital for assistance with data acquisition. We also thank Sam Solomon, Branka Spehar, Erin Goddard, and Kiley Seymour for comments on draft versions of the manuscript. This work was supported by an Australian Postgraduate Award to DM, an Australian Research Fellowship to CC, and by grants from the Australian Research Council and the National Health and Medical Research Council.

References

Appelle, S. Perception and discrimination as a function of stimulus orientation: the “oblique effect” in man and animals. *Psychol Bull 78*: 266–278, 1972.

Barlow, HB. Possible principles underlying the transformation of sensory messages. In: *Sensory Communication*, edited by **Rosenblith, WA**, Cambridge, MA: MIT Press, 217–234, 1961.

Brainard, DH. The psychophysics toolbox. *Spat Vis 10*: 433–436, 1997.

Bruce, ND, **Tsotsos, JK**. A statistical basis for visual field anisotropies. *Neurocomputing 69*: 1301–1304, 2006.

Clifford, CW, **Mannion, DJ**, **McDonald, JS**. Radial biases in the processing of motion and motion-defined contours by human visual cortex. *J Neurophysiol 102*: 2974–2981, 2009.

Coppola, DM, **Purves, HR**, **McCoy, AN**, **Purves, D**. The distribution of oriented contours in the real world. *Proc Natl Acad Sci USA 95*: 4002–4006, 1998.

Dan, Y, **Atick, JJ**, **Reid, RC**. Efficient coding of natural scenes in the lateral geniculate nucleus: experimental test of a computational theory. *J Neurosci 16*: 3351–3362, 1996.

DeYoe, EA, **Carman, GJ**, **Bandettini, P**, **Glickman, S**, **Wieser, J**, **Cox, R**, **Miller, D**, **Neitz, J**. Mapping striate and extrastriate visual areas in human cerebral cortex. *Proc Natl Acad Sci USA 93*: 2382–2386, 1996.

Dragoi, V, **Turcu, CM**, **Sur, M**. Stability of cortical responses and the statistics of natural scenes. *Neuron 32*: 1181–1192, 2001.

Engel, SA, **Glover, GH**, **Wandell, BA**. Retinotopic organization in human visual cortex and the spatial precision of functional MRI. *Cereb Cortex 7*: 181–192, 1997.

Essock, EA, **DeFord, JK**, **Hansen, BC**, **Sinai, MJ**. Oblique stimuli are seen best (not worst!) in naturalistic broad-band stimuli: a horizontal effect. *Vision Res 43*: 1329–1335, 2003.

Essock, EA, **Haun, AM**, **Kim, YJ**. An anisotropy of orientation-tuned suppression that matches the anisotropy of typical natural scenes. *J Vis 9*: 1–15, 2009.

Field, DJ. Relations between the statistics of natural images and the response properties of cortical cells. *J Opt Soc Am A 4*: 2379–2394, 1987.

Furmanski, CS, **Engel, SA**. An oblique effect in human primary visual cortex. *Nat Neurosci 3*: 535–536, 2000.

Furmanski, CS, **Schluppeck, D**, **Engel, SA**. Learning strengthens the response of primary visual cortex to simple patterns. *Curr Biol 14*: 573–578, 2004.

Geisler, WS. Motion streaks provide a spatial code for motion direction. *Nature 400*: 65–69, 1999.

Hansen, BC, **Essock, EA**. A horizontal bias in human visual processing of orientation and its correspondence to the structural components of natural scenes. *J Vis 4*: 1044–1060, 2004.

Hansen, BC, **Essock, EA**. Anisotropic local contrast normalization: the role of stimulus orientation and spatial frequency bandwidths in the oblique and horizontal effect perceptual anisotropies. *Vision Res 46*: 4398–4415, 2006.

Hansen, BC, **Essock, EA**, **Zheng, Y**, **DeFord, JK**. Perceptual anisotropies in visual processing and their relation to natural image statistics. *Network 14*: 501–526, 2003.

Hansen, KA, **Kay, KN**, **Gallant, JL**. Topographic organization in and near human visual area V4. *J Neurosci 27*: 11896–11911, 2007.

Heeger, DJ. Normalization of cell responses in cat striate cortex. *Vis Neurosci 9*: 181–197, 1992.

Heeley, DW, **Timney, B**. Meridional anisotropies of orientation discrimination for sine wave gratings. *Vision Res 28*: 337–344, 1988.

Jenkins, B. Orientational anisotropy in the human visual system. *Percept Psychophys 37*: 125–134, 1985.

Kamitani, Y, **Tong, F**. Decoding the visual and subjective contents of the human brain. *Nat Neurosci 8*: 679–685, 2005.

Kay, KN, **Naselaris, T**, **Prenger, RJ**, **Gallant, JL**. Identifying natural images from human brain activity. *Nature 452*: 352–355, 2008.

Larsson, J, **Heeger, DJ**. Two retinotopic visual areas in human lateral occipital cortex. *J Neurosci 26*: 13128–13142, 2006.

Lee, DN. The optic flow field: the foundation of vision. *Philos Trans R Soc Lond B Biol Sci 290*: 169–179, 1980.

Leventhal, AG. Relationship between preferred orientation and receptive field position of neurons in cat striate cortex. *J Comp Neurol 220*: 476–483, 1983.

Levick, WR, **Thibos, LN**. Analysis of orientation bias in cat retina. *J Physiol 329*: 243–261, 1982.

Li, B, **Peterson, MR**, **Freeman, RD**. Oblique effect: a neural basis in the visual cortex. *J Neurophysiol 90*: 204–217, 2003.

Logothetis, NK. What we can do and what we cannot do with fMRI. *Nature 453*: 869–878, 2008.

Ludbrook, J. Multiple comparison procedures updated. *Clin Exp Pharmacol Physiol 25*: 1032–1037, 1998.

Manjòn, JV, **Lull, JJ**, **Carbonell-Caballero, J**, **Garca-Martì, G**, **Martì-Bonmatì, L**, **Robles, M**. A nonparametric MRI inhomogeneity correction method. *Med Image Anal 11*: 336–345, 2007.

Mannion, DJ, **McDonald, JS**, **Clifford, CWG**. Discrimination of the local orientation structure of spiral Glass patterns early in human visual cortex. *NeuroImage 46*: 511–515, 2009.

O'Carroll, DC, **Bidwell, NJ**, **Laughlin, SB**, **Warrant, EJ**. Insect motion detectors matched to visual ecology. *Nature 382*: 63–66, 1996.

Pelli, DG. The VideoToolbox software for visual psychophysics: transforming numbers into movies. *Spat Vis 10*: 437–442, 1997.

Raemaekers, M, **Lankheet, MJM**, **Moorman, S**, **Kourtzi, Z**, **Van Wezel, RJA**. Directional anisotropy of motion responses in retinotopic cortex. *Hum Brain Mapp 30*: 3970–3980, 2009.

Rothkopf, CA, **Weisswange, TH**, **Triesch, J**. Learning independent causes in natural images explains the spacevariant oblique effect. In: *2009 IEEE 8th International Conference on Development and Learning*, 2009, 1–6.

Rovamo, J, **Virsu, V**, **Laurinen, P**, **Hyvrinen, L**. Resolution of gratings oriented along and across meridians in peripheral vision. *Invest Ophthalmol Vis Sci 23*: 666–670, 1982.

Sasaki, Y, **Rajimehr, R**, **Kim, BW**, **Ekstrom, LB**, **Vanduffel, W**, **Tootell, RB**. The radial bias: a different slant on visual orientation sensitivity in human and nonhuman primates. *Neuron 51*: 661–670, 2006.

Schira, MM, **Wade, AR**, **Tyler, CW**. Two-dimensional mapping of the central and parafoveal visual field to human visual cortex. *J Neurophysiol 97*: 4284–4295, 2007.

Serences, JT, **Saproo, S**, **Scolari, M**, **Ho, T**, **Muftuler, LT**. Estimating the influence of attention on population codes in human visual cortex using voxel-based tuning functions. *NeuroImage 44*: 223–31, 2009.

Sereno, MI, **Dale, AM**, **Reppas, JB**, **Kwong, KK**, **Belliveau, JW**, **Brady, TJ**, **Rosen, BR**, **Tootell, RB**. Borders of multiple visual areas in humans revealed by functional magnetic resonance imaging. *Science 268*: 889–893, 1995.

Simoncelli, EP. Vision and the statistics of the visual environment. *Curr Opin Neurobiol 13*: 144–149, 2003.

Singh, KD, **Smith, AT**, **Greenlee, MW**. Spatiotemporal frequency and direction sensitivities of human visual areas measured using fMRI. *NeuroImage 12*: 550–564, 2000.

Swisher, JD, **Gatenby, JC**, **Gore, JC**, **Wolfe, BA**, **Moon, CH**, **Kim, SG**, **Tong, F**. Multiscale pattern analysis of orientation-selective activity in the primary visual cortex. *J Neurosci 30*: 325–330, 2010.

Teller, DY. Linking propositions. *Vision Res 24*: 1233–1246, 1984.

Teo, PC, **Sapiro, G**, **Wandell, BA**. Creating connected representations of cortical gray matter for functional MRI visualization. *IEEE Trans Med Imaging 16*: 852–863, 1997.

Vandenbussche, E, **Vogels, R**, **Orban, GA**. Human orientation discrimination: changes with eccentricity in normal and amblyopic vision. *Invest Ophthalmol Vis Sci 27*: 237–245, 1986.

Wandell, BA, **Dumoulin, SO**, **Brewer, AA**. Visual field maps in human cortex. *Neuron 56*: 366–383, 2007.

Webster, MA, **Miyahara, E**. Contrast adaptation and the spatial structure of natural images. *J Opt Soc Am A 14*: 2355–2366, 1997.

Westheimer, G. The distribution of preferred orientations in the peripheral visual field. *Vision Res 43*: 53–57, 2003a.

Westheimer, G. Meridional anisotropy in visual processing: implications for the neural site of the oblique effect. *Vision Res 43*: 2281–2289, 2003b.

Williams, LJ. The oblique effect: a new slant on things. *Percept Mot Skills 54*: 992–994, 1982.

Wilson, HR, **Loffler, G**, **Wilkinson, F**, **Thistlethwaite, WA**. An inverse oblique effect in human vision. *Vision Res 41*: 1749–1753, 2001.

Yacoub, E, **Harel, N**, **Ugurbil, K**. High-field fMRI unveils orientation columns in humans. *Proc Natl Acad Sci USA 105*: 10607–10612, 2008.

Yushkevich, PA, **Piven, J**, **Hazlett, HC**, **Smith, RG**, **Ho, S**, **Gee, JC**, **Gerig, G**. User-guided 3D active contour segmentation of anatomical structures: significantly improved efficiency and reliability. *NeuroImage 31*: 1116–1128, 2006.

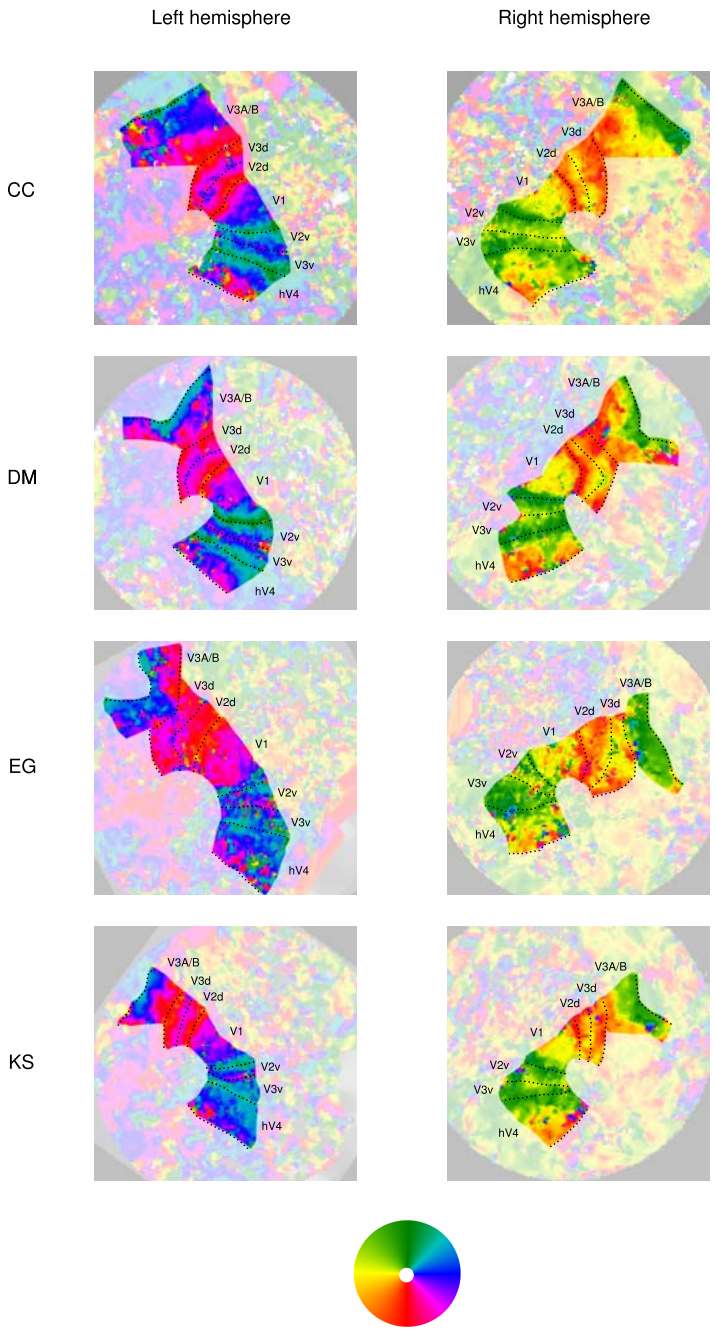

Supplementary Figure 1. Definitions of retinotopic visual areas for each subject. Shown are flattened representations of each hemisphere, which are coloured according to preferred visual field polar angle (for voxels with a coherence > 0.1). Dashed lines show the borders between identified visual areas.